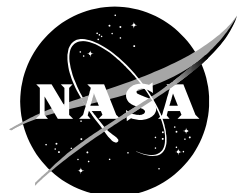


NASA/TM—2019—220477



TESS Data Release Notes: Sector 18, DR25

*Michael M. Fausnaugh, Christopher J. Burke
Kavli Institute for Astrophysics and Space Science, Massachusetts Institute of Technology,
Cambridge, Massachusetts*

*Douglas A. Caldwell
SETI Institute, Mountain View, California*

*Jon M. Jenkins
NASA Ames Research Center, Moffett Field, California*

*Jeffrey C. Smith, Joseph D. Twicken
SETI Institute, Mountain View, California*

*Roland Vanderspek
Kavli Institute for Astrophysics and Space Science, Massachusetts Institute of Technology,
Cambridge, Massachusetts*

*John P. Doty
Noqsi Aerospace Ltd, Billerica, Massachusetts*

*Eric B. Ting
Ames Research Center, Moffett Field, California*

*Joel S. Villasenor
Kavli Institute for Astrophysics and Space Science, Massachusetts Institute of Technology,
Cambridge, Massachusetts*

December 20, 2019

NASA STI Program ... in Profile

Since its founding, NASA has been dedicated to the advancement of aeronautics and space science. The NASA scientific and technical information (STI) program plays a key part in helping NASA maintain this important role.

The NASA STI program operates under the auspices of the Agency Chief Information Officer. It collects, organizes, provides for archiving, and disseminates NASA's STI. The NASA STI program provides access to the NTRS Registered and its public interface, the NASA Technical Reports Server, thus providing one of the largest collections of aeronautical and space science STI in the world. Results are published in both non-NASA channels and by NASA in the NASA STI Report Series, which includes the following report types:

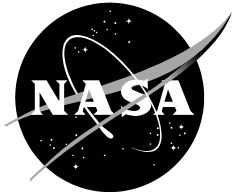
- **TECHNICAL PUBLICATION.** Reports of completed research or a major significant phase of research that present the results of NASA Programs and include extensive data or theoretical analysis. Includes compilations of significant scientific and technical data and information deemed to be of continuing reference value. NASA counterpart of peer-reviewed formal professional papers but has less stringent limitations on manuscript length and extent of graphic presentations.
- **TECHNICAL MEMORANDUM.** Scientific and technical findings that are preliminary or of specialized interest, e.g., quick release reports, working papers, and bibliographies that contain minimal annotation. Does not contain extensive analysis.
- **CONTRACTOR REPORT.** Scientific and technical findings by NASA-sponsored contractors and grantees.

- **CONFERENCE PUBLICATION.** Collected papers from scientific and technical conferences, symposia, seminars, or other meetings sponsored or co-sponsored by NASA.
- **SPECIAL PUBLICATION.** Scientific, technical, or historical information from NASA programs, projects, and missions, often concerned with subjects having substantial public interest.
- **TECHNICAL TRANSLATION.** English-language translations of foreign scientific and technical material pertinent to NASA's mission.

Specialized services also include organizing and publishing research results, distributing specialized research announcements and feeds, providing information desk and personal search support, and enabling data exchange services.

For more information about the NASA STI program, see the following:

- Access the NASA STI program home page at <http://www.sti.nasa.gov>
- E-mail your question to help@sti.nasa.gov
- Phone the NASA STI Information Desk at 757-864-9658
- Write to:
NASA STI Information Desk
Mail Stop 148
NASA Langley Research Center
Hampton, VA 23681-2199



TESS Data Release Notes: Sector 18, DR25

*Michael M. Fausnaugh, Christopher J. Burke
Kavli Institute for Astrophysics and Space Science, Massachusetts Institute of Technology,
Cambridge, Massachusetts*

*Douglas A. Caldwell
SETI Institute, Mountain View, California*

*Jon M. Jenkins
NASA Ames Research Center, Moffett Field, California*

*Jeffrey C. Smith, Joseph D. Twicken
SETI Institute, Mountain View, California*

*Roland Vanderspek
Kavli Institute for Astrophysics and Space Science, Massachusetts Institute of Technology,
Cambridge, Massachusetts*

*John P. Doty
Noqi Aerospace Ltd, Billerica, Massachusetts*

*Eric B. Ting
Ames Research Center, Moffett Field, California*

*Joel S. Villaseñor
Kavli Institute for Astrophysics and Space Science, Massachusetts Institute of Technology,
Cambridge, Massachusetts*

Acknowledgements

These Data Release Notes provide information on the processing and export of data from the Transiting Exoplanet Survey Satellite (TESS). The data products included in this data release are full frame images (FFIs), target pixel files, light curve files, collateral pixel files, cotrending basis vectors (CBVs), and Data Validation (DV) reports, time series, and associated xml files.

These data products were generated by the TESS Science Processing Operations Center (SPOC, [Jenkins et al., 2016](#)) at NASA Ames Research Center from data collected by the TESS instrument, which is managed by the TESS Payload Operations Center (POC) at Massachusetts Institute of Technology (MIT). The format and content of these data products are documented in the [Science Data Products Description Document \(SDPDD\)](#)¹. The SPOC science algorithms are based heavily on those of the Kepler Mission science pipeline, and are described in the Kepler Data Processing Handbook ([Jenkins, 2017](#)).² The Data Validation algorithms are documented in [Twicken et al. \(2018\)](#) and [Li et al. \(2019\)](#). The [TESS Instrument Handbook](#) ([Vanderspek et al., 2018](#)) contains more information about the TESS instrument design, detector layout, data properties, and mission operations.

The TESS Mission is funded by NASA's Science Mission Directorate.

This report is available in electronic form at
<https://archive.stsci.edu/tess/>

¹<https://archive.stsci.edu/missions/tess/doc/EXP-TESS-ARC-ICD-TM-0014.pdf>

²<https://archive.stsci.edu/kepler/manuals/KSCI-19081-002-KDPH.pdf>

1 Observations

TESS Sector 18 observations include physical orbits 43 and 44 of the spacecraft around the Earth. Data collection was paused for 1.00 days during perigee passage while downloading data. The spacecraft passed through the shadow of the Earth at the start of orbit 43. During this time, the instrument was turned off and no data were collected for 6.2 hours between TJD 1791.1115 and 1791.3699. The thermal state of the spacecraft changed during this time, and trends in the raw photometry and target positions are apparent after data collection resumed. In total, there are 23.12 days of science data collected in Sector 18.

Table 1: Sector 18 Observation times

	UTC	TJD ^a	Cadence #
Orbit 43 start	2019-11-03 03:35:25	1790.65111	405501
Instrument shutdown for eclipse	2019-11-03 14:39:24	1791.11150	405833
Instrument restart	2019-11-03 20:51:30	1791.36989	406019
Orbit 43 end	2019-11-14 22:31:25	1802.43999	413989
Orbit 44 start	2019-11-15 22:35:25	1803.44277	414711
Orbit 44 end	2019-11-27 12:41:24	1815.03026	423054

^a TJD = TESS JD = JD - 2,457,000.0

The spacecraft was pointing at RA (J2000): 16.1103°; Dec (J2000): 67.9575°; Roll: 40.5453°. Two-minute cadence data were collected for 20,000 targets, and full frame images were collected every 30 minutes. See the TESS project [Sector 18 observation page](#)³ for the coordinates of the spacecraft pointing and center field-of-view of each camera, as well as the detailed target list. Fields-of-view for each camera and the Guest Investigator two-minute target list can be found at the TESS Guest Investigator Office [observations status page](#)⁴.

1.1 Notes on Individual Targets

Two bright stars ($T_{\text{mag}} \lesssim 1.8$) with large pixel stamps were not processed in the photometric pipeline. Target pixel files with raw data are provided, but no light curves were produced. The affected TIC IDs are 186744198 and 292057658.

Seven target stars (101255849, 279979429, 334487469, 341873045, 354379201, 441804565, 2022481918) are blended with comparably bright stars—the contaminating flux for these objects is very large, and the resulting photometry for such targets is expected to be unreliable.

One target star (445258198, $T_{\text{mag}} = 5.92$) lies within the same pixel of a very bright star (445258206, $T_{\text{mag}} = 2.8$). In this case, no optimal aperture was assigned. A target pixel file with raw data is provided, but no light curve was produced.

Two targets (431863107 and 441804565) had a pixel stamp that did not fully capture the bleed trails.

³<https://tess.mit.edu/observations/sector-18>

⁴<https://heasarc.gsfc.nasa.gov/docs/tess/status.html>

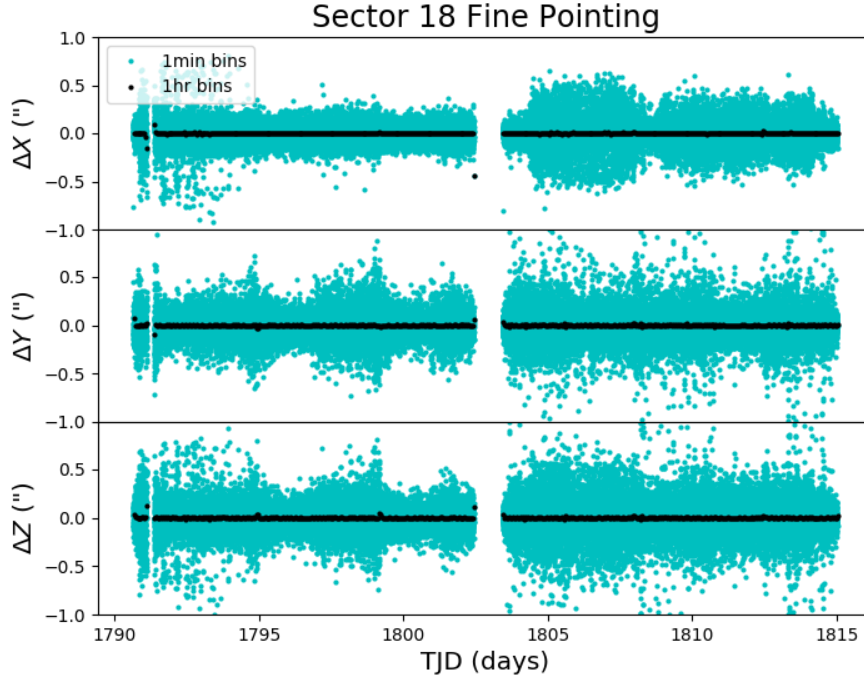


Figure 1: Guiding corrections based on spacecraft fine pointing telemetry. The delta-quaternions from each camera have been converted to spacecraft frame, binned to 1 minute and 1 hour, and averaged across cameras. Long-term trends (such as those caused by differential velocity aberration) have also been removed. The $\Delta X/\Delta Y$ directions represent offsets along the detectors’ rows/columns, while the ΔZ direction represents spacecraft roll. The gap at the start of the sector is due to the instrument shut-down during the eclipse.

1.2 Spacecraft Pointing and Momentum dumps

Camera 4 alone was used for guiding in orbit 43, and both Camera 1 and Camera 4 were used for guiding in orbit 44. The reaction wheel speeds were reset with momentum dumps every 4.25 days (orbit 43) or 4.5 days (orbit 44). Figure 1 summarizes the pointing performance over the course of the sector based on Fine Pointing telemetry. The gap at the start of the sector is due to the instrument shut-down during the eclipse.

1.3 Scattered Light

Figure 2 shows the median value of the background estimate for all targets on a given CCD as a function of time. Figure 3 shows the angle between each camera’s boresight and the Earth or Moon—this figure can be used to identify periods affected by scattered light and the relative contributions of the Earth and Moon to the image backgrounds.

In Sector 18, the Moon and Earth move close enough to the field of view of Camera 1 at the end of orbit 43 to briefly saturate the detector.

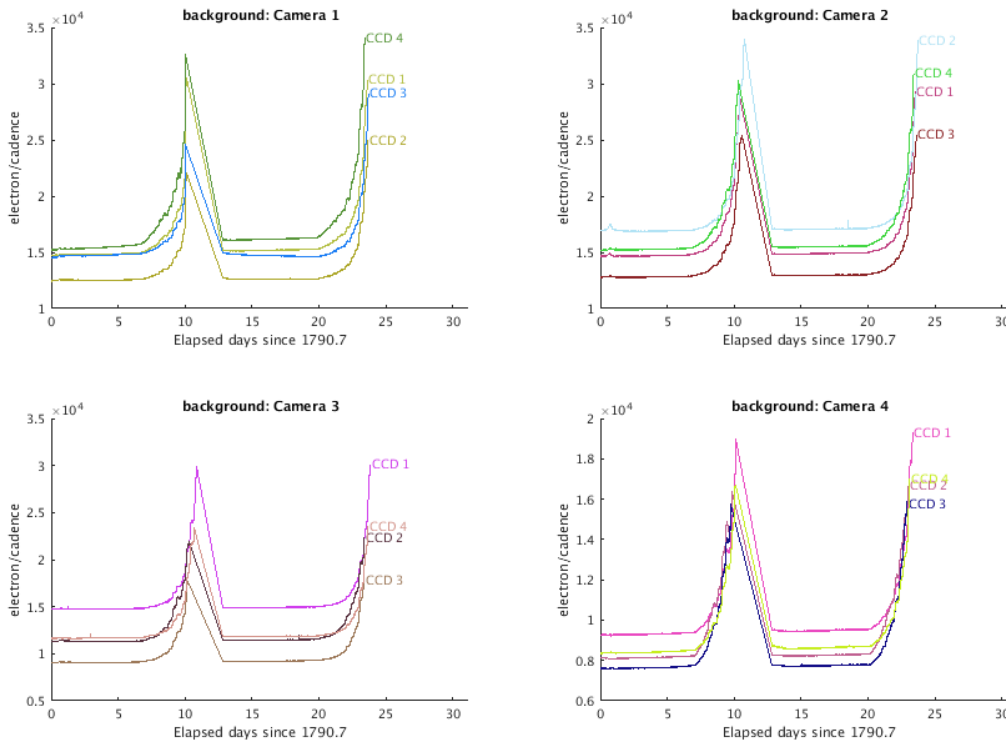


Figure 2: Median background flux across all targets on a given CCD in each camera. The changes are caused by variations in the orientation and distance of the Earth and Moon.

2 Data Anomaly Flags

See the [SDPDD](#) (§9) for a list of data quality flags and the associated binary values used for TESS data, and the [TESS Instrument Handbook](#) for a more detailed description of each flag.

The following flags were not used in Sector 18: bits 1, 2, 7, 9, and 11 (Attitude Tweak, Safe Mode, Cosmic Ray in Aperture, Discontinuity, Cosmic Ray in Collateral Pixel).

Cadences marked with bits 3, 4, 6, and 12 (Coarse Point, Earth Point, Reaction Wheel Desaturation Event, and Straylight) were marked based on spacecraft telemetry. Note that the Straylight flag (bit 12) marks periods for when certain cameras are not suitable for guiding and do not necessarily indicate problematic data for other cameras. We suggest that users inspect the light curves before removing data in their analyses when this bit is set.

Cadences marked with bit 5 and 10 (Argabrightening Events and Impulsive Outlier) were identified by the SPOC pipeline. Bit 5 marks a sudden change in the background measurements. In practice, bit 5 flags are caused by rapidly changing glints and unstable pointing at times near momentum dumps. Bit 10 marks an outlier identified by PDC and omitted from the cotrending procedure.

Cadences marked with bit 8 (Manual Exclude) are ignored by PDC, TPS, and DV for cotrending and transit searches. In Sector 18, these cadences were identified using spacecraft

Earth/Moon angles for Sector 18 (O43 + O44), Ed. Dec. = +54
 2019-11-02 07:47:00 to 2019-11-27 23:05:00 UTC

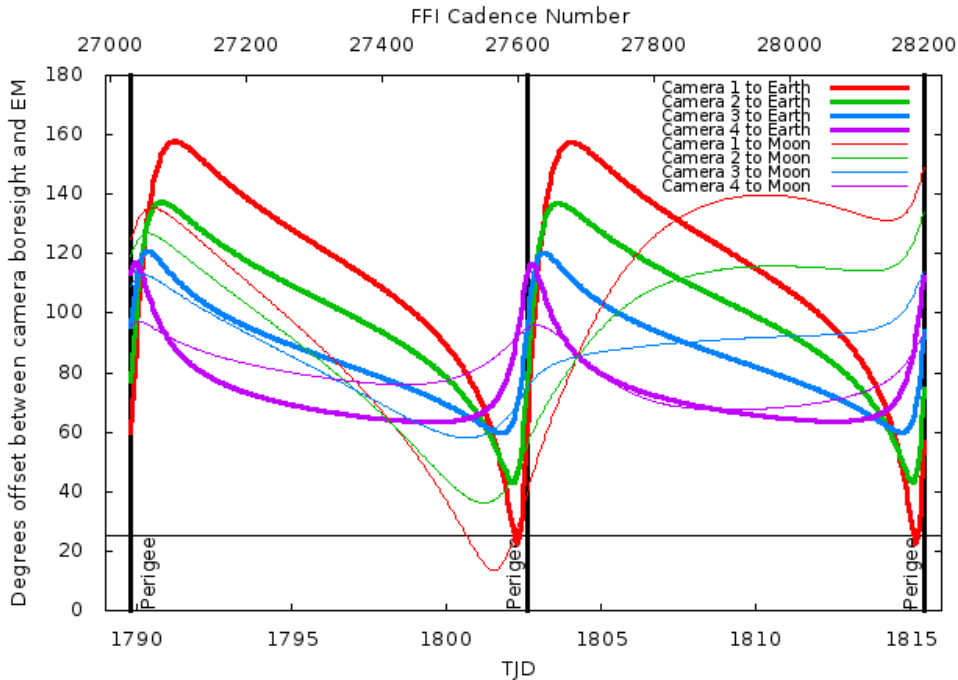


Figure 3: Angle between the four camera boresights and the Earth/Moon as a function of time. When the Earth is within $\sim 25^\circ$ of a camera’s boresight, transiting planet searches may be compromised by high levels of scattered light. At larger angles, up to $\sim 35^\circ$, scattered light patterns and complicated structures may be visible. At yet larger angles, low level patchy features may be visible. Scattered light from the Moon is generally only noticeable below $\sim 35^\circ$. This figure can be used to identify periods affected by scattered light and the relative contributions of the Earth and Moon to the background. However, the background intensity and locations of scattered light features depend on additional factors, such as the Earth/Moon azimuth and distance from the spacecraft.

telemetry from the fine pointing system. All cadences with pointing excursions >7 arcseconds (~ 0.3 pixel) were flagged for manual exclude. See Figure 4 for an assessment of the performance of the cotrending based on the final set of manual excludes.

In Sector 18, bit 13 (value 4096, “Scattered Light”) was set based on the observed background measurements for targets on each CCD, in order to mask cadences that would negatively affect the systematic error removal in PDC and the planet search in TPS.

FFIs were only marked with bits 3, 6 and 12 (Course Point, Reaction Wheel Desaturation Events and Straylight). Only one FFI is affected by each momentum dump. There are no WCS coordinates for FFIs that coincide with momentum dumps.

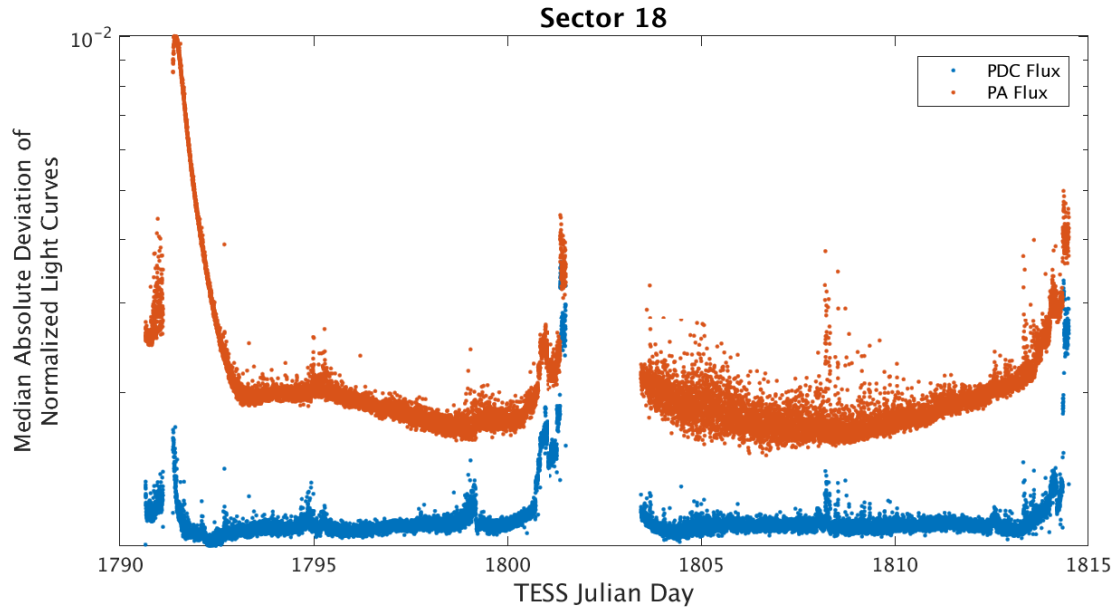


Figure 4: Median absolute deviation (MAD) for the 2-minute cadence data from Sector 18, showing the performance of the cotrending after identifying Manual Exclude data quality flags. The MAD is calculated in each cadence across stars with flux variations less than 1% for both the PA (red) and PDC (blue) light curves, where each light curve is normalized by its median flux value. The scatter in the PA light curves is much higher than that for the PDC light curves, and the outliers in the PA light curves are largely absent from the PDC light curves due to the use of the anomaly flags.

3 Anomalous Effects

3.1 Smear Correction Issues

The following columns were impacted by a bright star in the upper buffer row that bleeds into the upper serial register resulting in an overestimated smear correction. In addition, the first target listed leads to smear contamination by being located on the last row of the science frame.

- Camera 4, CCD 1, Column 1117, Star AC Draconis
- Camera 4, CCD 2, Column 591, Star HD 159712
- Camera 4, CCD 3, Column 354, Star HD 147202

3.2 Fireflies and Fireworks

Table 2 lists all firefly and fireworks events for Sector 18. These phenomena are small, spatially extended, comet-like features in the images—created by sunlit particles in the camera FOV—that may appear one or two at a time (fireflies) or in large groups (fireworks). See the [TESS Instrument Handbook](#) for a more complete description.

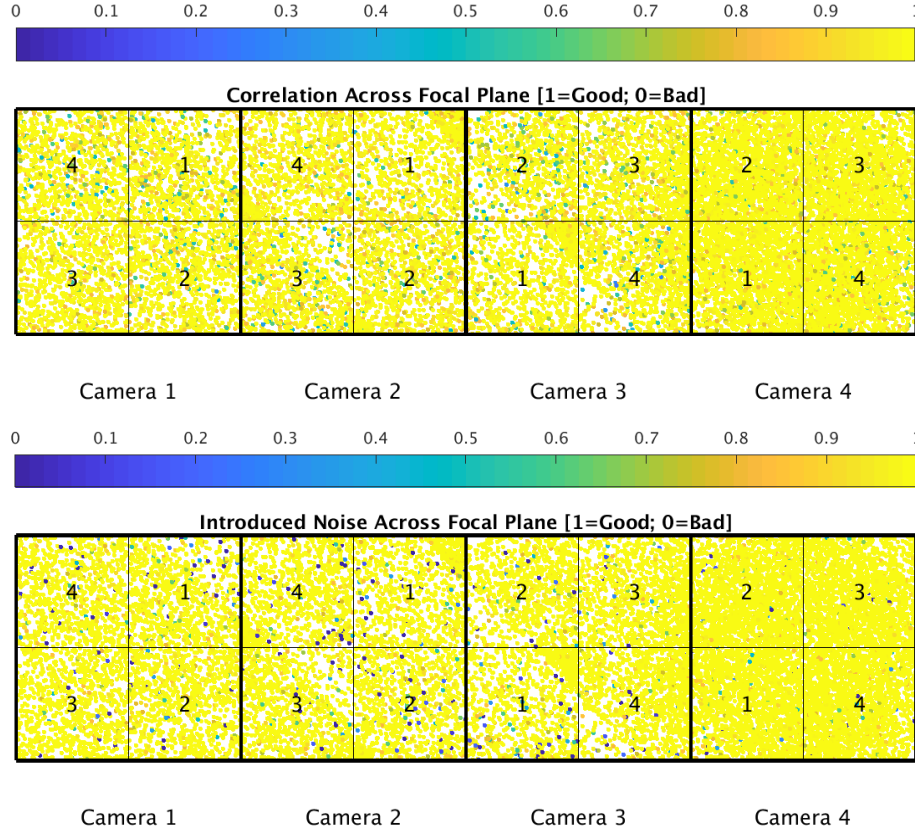


Figure 5: PDC residual correlation goodness metric (top panel) and PDC introduced noise goodness metric (bottom panel). The metric values are shown on a focal plane map indicating the camera and CCD location of each target. The correlation goodness metric is calibrated such that a value greater than 0.8 means there is less than 10% mean absolute correlation between the target under study and all other targets on the CCD. The introduced noise metric is calibrated such that a value greater than 0.8 means the power in broad-band introduced noise is below the level of uncertainties in the flux values.

3.3 Corrections to Data Product Timestamps

In Sector 18, we found an error in the FFI timestamps. The readouts of the four cameras are staggered by 0.5 seconds in the following order: Camera 1 (0 second offset), Camera 3 (0.5 second offset), Camera 4 (1.0 second offset), and Camera 2 (1.5 second offset). Although these offsets are correctly incorporated into the timestamps in the target pixel files and light curves, the FFI time stamps are not corrected for the staggered readout. This issue will be corrected in future sectors. For Sector 1 through Sector 18, the offsets for each camera can be added to the TSTART and TSTOP header values in the FFIs to correct the issue. Note that there are additional millisecond offsets for each CCD relative to the camera as a whole, though these offsets are smaller than the absolute accuracy of the timestamps (± 50 ms). It should also be noted that although the Camera- and CCD-specific readout offsets are not added to the TSTART and TSTOP header values, the readout offset is correctly identified by the TMOFST $_{mn}$ header value where m is the Camera number and n is the CCD number

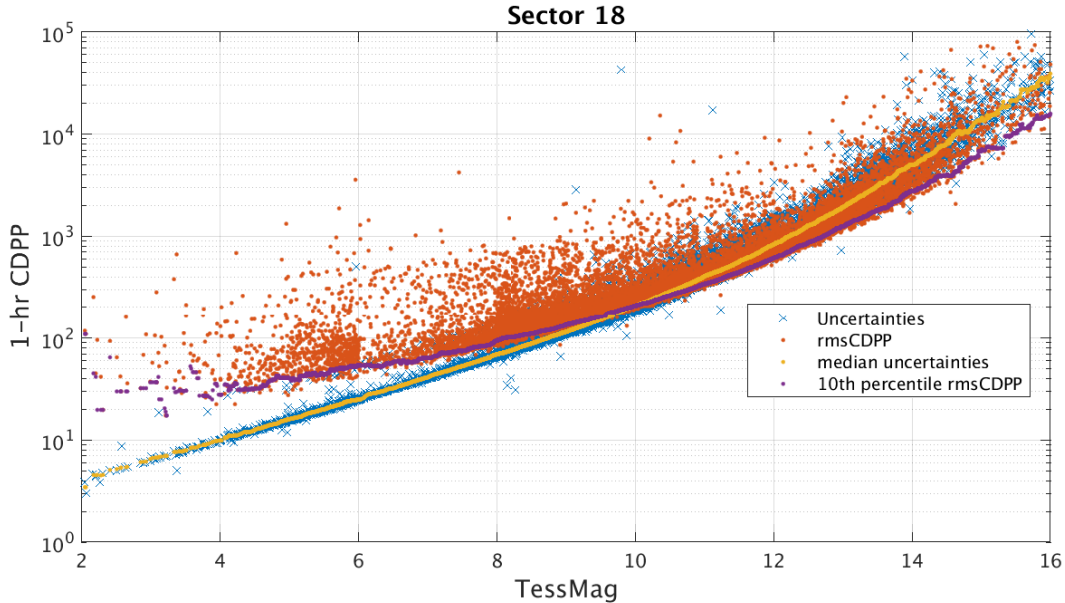


Figure 6: 1-hour CDPP. The red points are the RMS CDPP measurements for the 19997 light curves from Sector 18 plotted as a function of TESS magnitude. The blue x’s are the uncertainties, scaled to 1-hour timescale. The purple curve is a moving 10th percentile of the RMS CDPP measurements, and the gold curve is a moving median of the 1-hr uncertainties.

associated with the given FFI or target.

In addition, the TSTOP header values in the target pixel files, light curve files, and FFIs are overestimated by 20 ms, and the TIME column of the target pixel files and light curve files are overestimated by 10 ms. This issue will be corrected in future sectors.

4 Pipeline Performance and Results

4.1 Light Curves and Photometric Precision

Figure 5 gives the PDC goodness metrics for residual correlation and introduced noise on a scale between 0 (bad) and 1 (good). The performance of PDC is very good and generally uniform over most of the field of view. Figure 6 shows the achieved Combined Differential Photometric Precision (CDPP) at 1-hour timescales for all targets.

The thermal state of the spacecraft changed during the instrument shutoff at the time of the eclipse, and trends in the raw photometry and target positions are apparent after data collection resumed. However, the pipeline effectively removes these trends in the PDC light curves.

4.2 Transit Search and Data Validation

In Sector 18, the light curves of 19997 targets were subjected to the transit search in TPS. Of these, Threshold Crossing Events (TCEs) at the 7.1σ level were generated for 630 targets.

Table 2: Sector Fireflies and Fireworks

FFI Start	FFI End	Cameras	Description
2019307232925	2019307235925	4	Firefly
2019308062925	2019308072925	2,3	Firefly
2019308085925	2019308092925	2,3	Fireflies
2019310005925	2019310012925	1	Firefly
2019310025925	2019310032925	3	Firefly
2019311025925	2019311032925	1	Firefly
2019316155925	2019316162925	1	Firefly
2019322042925	2019322045925	4	Firefly
2019325145925	2019325152925	2,3	Fireflies
2019326062925	2019326065925	1,3	Fireflies
2019330012925	2019330015925	2	Firefly

We employed an iterative method when conducting the Sector 18 transit search. The top panel of Figure 7 shows the number of TCEs at a given cadence that exhibit a transit signal from an initial run of TPS. The 3σ peaks were used to define deemphasis weights for a second run of TPS, the results of which are shown in the bottom panel of Figure 7. The final set of TCEs and the results reported here are based on the second run of TPS. The values of the adopted deemphasis weights are provided in the DV timeseries data products for targets with TCEs.

The top panel of Figure 8 shows the distribution of orbital periods for the final set of TCEs found in Sector 18. The vertical histogram in the right panel of Figure 8 shows the distribution of transit depths derived from limb-darkened transiting planet model fits for TCEs. The model transit depths range down to the order of 100 ppm, but the bulk of the transit depths are considerably larger.

A search for additional TCEs in potential multiple planet systems was conducted in DV through calls to TPS. A total of 915 TCEs were ultimately identified in the SPOC pipeline on 630 unique target stars. Table 3 provides a breakdown of the number of TCEs by target. Note that targets with large numbers of TCEs are likely to include false positives.

Table 3: Sector 18 TCE Numbers

Number of TCEs	Number of Targets	Total TCEs
1	402	402
2	178	356
3	45	135
4	3	12
5	2	10
–	630	915

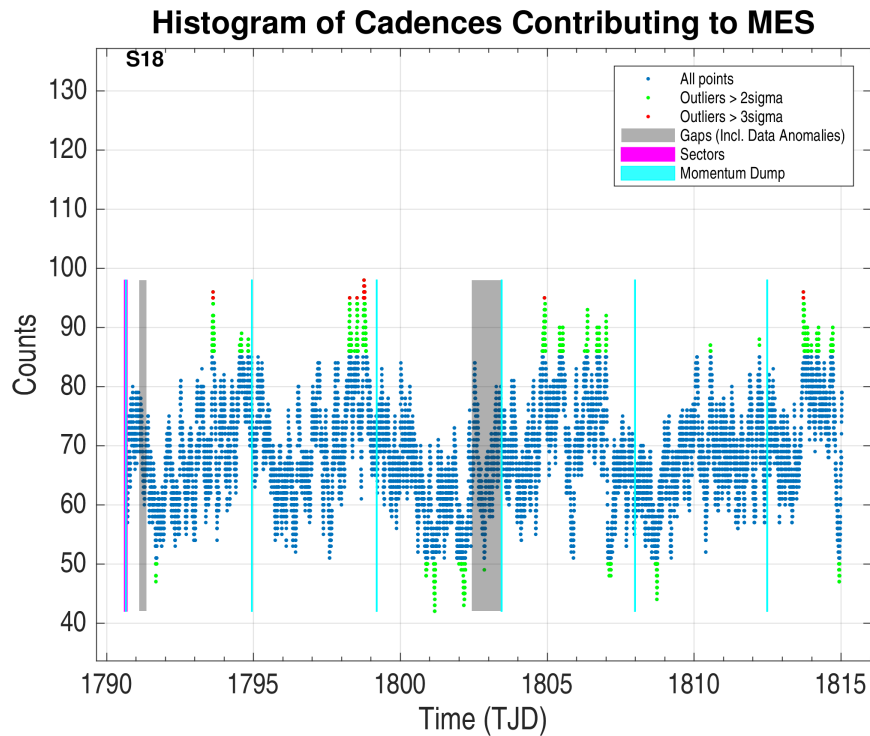
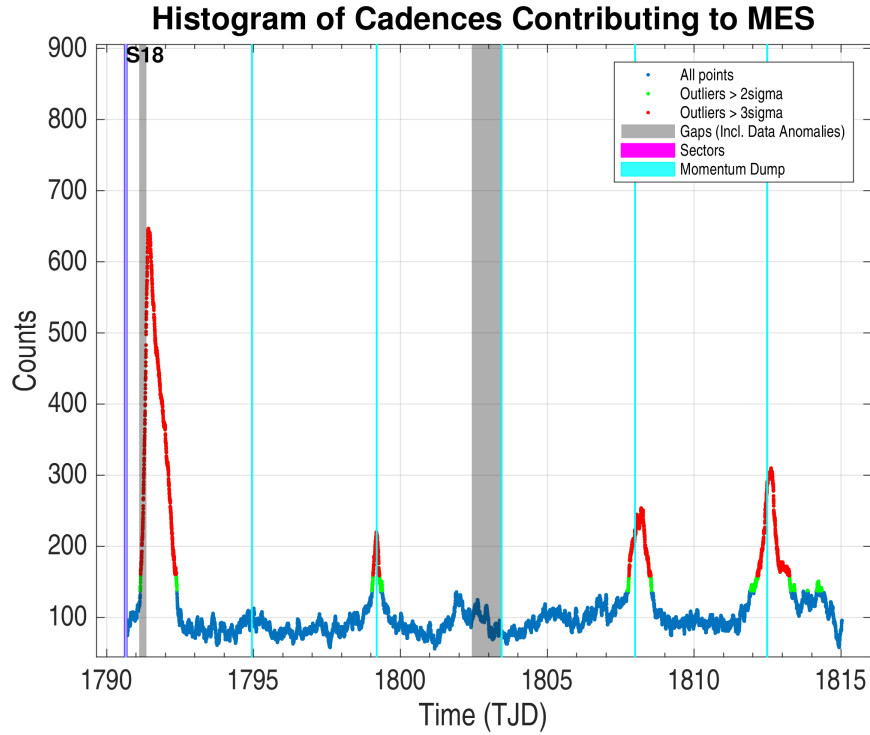


Figure 7: Top panel: Number of TCEs at a given cadence exhibiting a transit signal, based on an initial run of TPS. Any isolated peaks are caused by single events that result in spurious TCEs. These peaks were used to define deemphasis weights that suppress problematic epochs for the transit detection statistics in a second iteration of TPS. Bottom panel: Results from the second run of TPS.

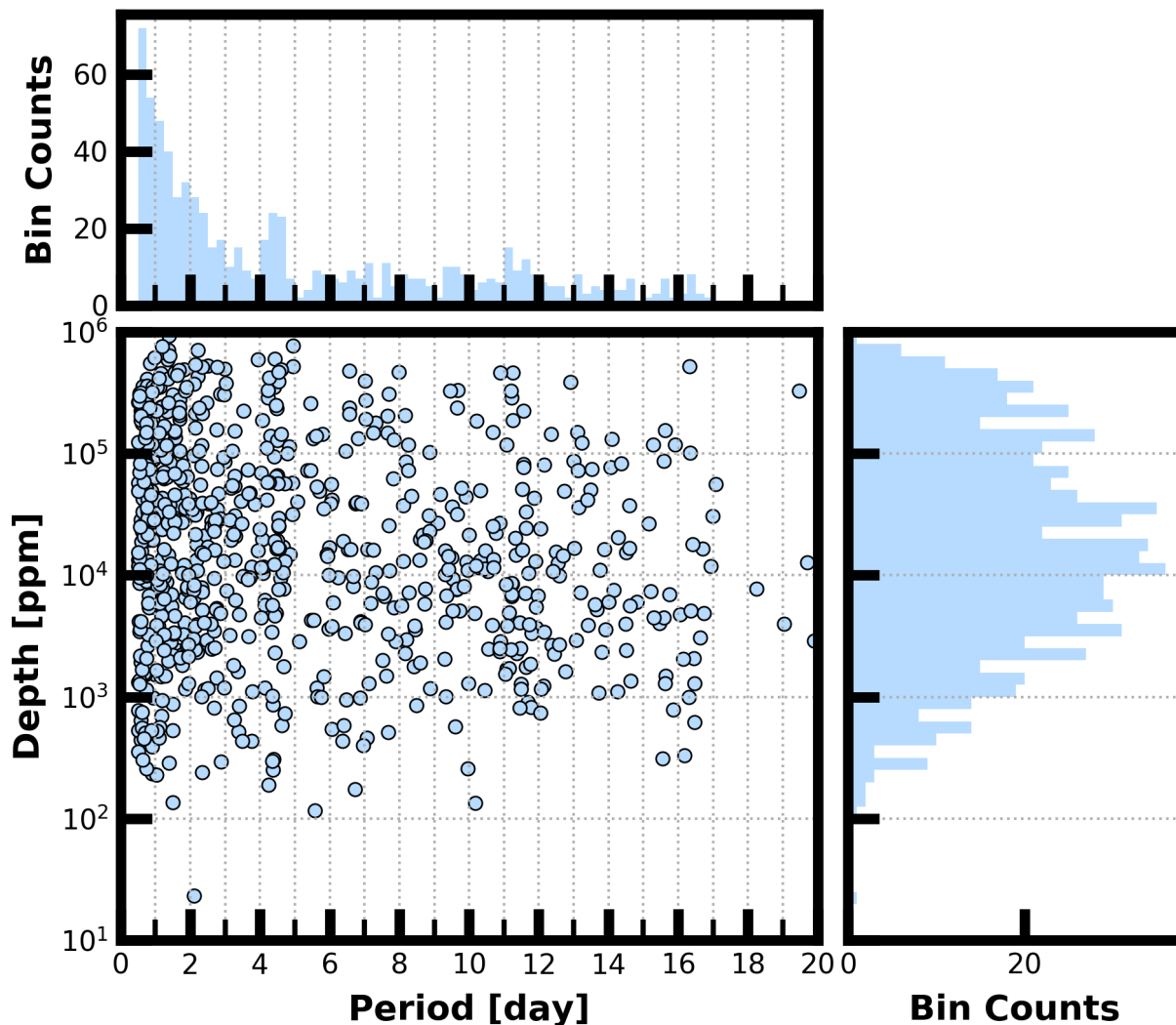


Figure 8: Lower Left Panel: Transit depth as a function of orbital period for the 915 TCEs identified for the Sector 18 search. For enhanced visibility of long period detections, TCEs with orbital period <0.5 days are not shown. Reported depth comes from the DV limb darkened transit fit depth when available, and the DV trapezoid model fit depth when not available. Top Panel: Orbital period distribution of the TCEs shown in the lower left panel. Right Panel: Transit depth distribution for the TCEs shown in the lower left panel.

References

- Jenkins, J. M. 2017, [Kepler Data Processing Handbook](#): Overview of the Science Operations Center, Tech. rep., NASA Ames Research Center
- Jenkins, J. M., Twicken, J. D., McCauliff, S., et al. 2016, in Proc. SPIE, Vol. 9913, Software and Cyberinfrastructure for Astronomy IV, [99133E](#)
- Li, J., Tenenbaum, P., Twicken, J. D., et al. 2019, *PASP*, 131, 024506, doi: [10.1088/1538-3873/aaf44d](#)
- Twicken, J. D., Catanzarite, J. H., Clarke, B. D., et al. 2018, *PASP*, 130, 064502, doi: [10.1088/1538-3873/aab694](#)
- Vanderspek, R., Doty, J., Fausnaugh, M., et al. 2018, [TESS Instrument Handbook](#), Tech. rep., Kavli Institute for Astrophysics and Space Science, Massachusetts Institute of Technology

Acronyms and Abbreviation List

BTJD	Barycentric-corrected TESS Julian Date
CAL	Calibration Pipeline Module
CBV	Cotrending Basis Vector
CCD	Charge Coupled Device
CDPP	Combined Differential Photometric Precision
COA	Compute Optimal Aperture Pipeline Module
CSCI	Computer Software Configuration Item
CTE	Charge Transfer Efficiency
Dec	Declination
DR	Data Release
DV	Data Validation Pipeline Module
DVA	Differential Velocity Aberration
FFI	Full Frame Image
FIN	FFI Index Number
FITS	Flexible Image Transport System
FOV	Field of View
FPG	Focal Plane Geometry model
KDPH	Kepler Data Processing Handbook
KIH	Kepler Instrument Handbook
KOI	Kepler Object of Interest
MAD	Median Absolute Deviation
MAP	Maximum A Posteriori
MAST	Mikulski Archive for Space Telescopes
MES	Multiple Event Statistic
NAS	NASA Advanced Supercomputing Division
PA	Photometric Analysis Pipeline Module

PDC Pre-Search Data Conditioning Pipeline Module
PDC-MAP Pre-Search Data Conditioning Maximum A Posteriori algorithm
PDC-msMAP Pre-Search Data Conditioning Multiscale Maximum A Posteriori algorithm
PDF Portable Document Format
POC Payload Operations Center
POU Propagation of Uncertainties
ppm Parts-per-million
PRF Pixel Response Function
RA Right Ascension
RMS Root Mean Square
SAP Simple Aperture Photometry
SDPDD Science Data Product Description Document
SNR Signal-to-Noise Ratio
SPOC Science Processing Operations Center
SVD Singular Value Decomposition
TCE Threshold Crossing Event
TESS Transiting Exoplanet Survey Satellite
TIC TESS Input Catalog
TIH TESS Instrument Handbook
TJD TESS Julian Date
TOI TESS Object of Interest
TPS Transiting Planet Search Pipeline Module
UTC Coordinated Universal Time
WCS World Coordinate System
XML Extensible Markup Language